

## Phase-space visualization of a metal-insulator transition

**Christian Aulbach, André Wobst, Gert-Ludwig Ingold, Peter Hänggi, Imre Varga**

### Angaben zur Veröffentlichung / Publication details:

Aulbach, Christian, André Wobst, Gert-Ludwig Ingold, Peter Hänggi, and Imre Varga. 2004. "Phase-space visualization of a metal-insulator transition." *New Journal of Physics* 6: 70. <https://doi.org/10.1088/1367-2630/6/1/070>.

## Phase-space visualization of a metal–insulator transition

To cite this article: Christian Aulbach *et al* 2004 *New J. Phys.* **6** 70

View the [article online](#) for updates and enhancements.

### Related content

- [Localization of weakly interacting Bose gas in quasiperiodic potential](#)  
Sayak Ray, Mohit Pandey, Anandamohan Ghosh *et al.*
- [Exponential localization in one-dimensional quasi-periodic optical lattices](#)  
Michele Modugno
- [Anderson localization in Bose–Einstein condensates](#)  
Giovanni Modugno

### Recent citations

- [Drive-induced delocalization in the Aubry-André model](#)  
S. Ray *et al*
- [A finite temperature study of ideal quantum gases in the presence of one dimensional quasi-periodic potential](#)  
Nilanjan Roy and Subhasis Sinha
- [Bosons with incommensurate potential and spin-orbit coupling](#)  
Sayak Ray *et al*

## Phase-space visualization of a metal–insulator transition

Christian Aulbach<sup>1</sup>, André Wobst<sup>1</sup>, Gert-Ludwig Ingold<sup>1</sup>,  
Peter Hänggi<sup>1</sup> and Imre Varga<sup>2</sup>

<sup>1</sup> Institut für Physik, Universität Augsburg, Universitätsstraße 1,  
D-86135 Augsburg, Germany

<sup>2</sup> Elméleti Fizika Tanszék, Fizikai Intézet, Budapesti Műszaki és  
Gazdaságtudományi Egyetem, H-1521 Budapest, Hungary

E-mail: [Gert.Ingold@physik.uni-augsburg.de](mailto:Gert.Ingold@physik.uni-augsburg.de)

*New Journal of Physics* **6** (2004) 70

Received 12 May 2004

Published 5 July 2004

Online at <http://www.njp.org/>

doi:10.1088/1367-2630/6/1/070

**Abstract.** The Aubry–André model with its transition from a delocalized to a localized phase in one dimension is particularly well suited for a phase-space study of such a metal–insulator transition. The dependence of the Husimi function on the potential strength is discussed and described quantitatively by means of marginal distributions and the inverse participation ratio in phase space. The phase-space representation not only helps to visualize the metal–insulator transition but also sheds light on the question why such a transition is possible in a one-dimensional system. Differences and similarities between the Aubry–André model and the Anderson model in one and higher dimensions, respectively, will be pointed out.

### Contents

1. <b>Introduction</b>	2
2. <b>Aubry–André model</b>	2
3. <b>Phase-space concepts</b>	6
4. <b>Aubry–André model in phase space</b>	9
5. <b>Conclusion</b>	15
<b>Acknowledgments</b>	16
<b>References</b>	16

## 1. Introduction

Recently, it has been argued that phase-space methods may represent a useful tool to analyse models in condensed matter physics [1]. Such an approach allows to treat real and momentum space on an equal footing and thus provides a consistent description of different transport regimes. Two phase-space methods have been devised to characterize the phase-space properties of quantum states. Starting from a positive-definite phase-space distribution, the so-called Husimi distribution function [2, 3], the Wehrl entropy [1] and an inverse participation ratio in phase space [4]–[7] have been employed. An alternative approach is based on the marginal distributions of the Husimi distribution function [8].

These works have mostly been devoted to the study of the Anderson model of disordered systems [9] in up to three dimensions, which allows to relate well-known features of the model to the corresponding phase-space properties. Unfortunately, it is only in two and higher dimensions that the Anderson model exhibits a variety of transport regimes comprising ballistic, diffusive and localized regimes. Dimensions larger than 2 are required for the Anderson transition to occur, which separates a metallic from an insulating phase. Such high dimensions preclude a straightforward visualization of the phase-space density and thus an appealing feature of this approach is lost. Furthermore, the required numerical efforts restrict the calculations to rather small system sizes so that it is difficult to deduce results valid in the thermodynamic limit. It is therefore desirable to study a model, which already in one dimension, gives rise to a non-trivial behaviour.

The Aubry–André model [10] displays a localization transition in one dimension and is therefore ideally suited for our purposes. A comparison between the Anderson model and the Aubry–André model on the basis of phase-space methods has recently allowed to gain additional insight into the mechanism of the delocalization–localization transition in these models. The nature of the coupling between different plane waves through a weak potential was identified as being crucial for the existence of such a phase transition [5]. In the following, we give a more detailed discussion of the Aubry–André model and will employ the Husimi function to visualize important aspects of the model in phase space.

## 2. Aubry–André model

The almost Mathieu operator [11]

$$H = \sum_n (|n\rangle\langle n+1| + |n+1\rangle\langle n|) + \lambda \sum_n \cos(2\pi\beta n) |n\rangle\langle n| \quad (1)$$

considered within the Aubry–André model can be viewed as describing the motion of a particle on a one-dimensional lattice where  $|n\rangle$  is a Wannier state at lattice site  $n$ . The Hamiltonian  $H$  depends on two parameters, namely the potential strength  $\lambda$  taken in units of the hopping matrix element and the period of the potential determined by  $\beta$ .

For  $\lambda = 2$ , it was demonstrated by Harper [12] that the Hamiltonian (1) describes an electron on a square lattice in a perpendicular magnetic field, a situation first discussed by Peierls [13]. In this case, the parameter  $\beta = \Phi/\Phi_0$  corresponds to the flux  $\Phi$  per plaquette in units of the flux quantum  $\Phi_0 = h/e$ . It was found by Hofstadter [14] that the character of the eigenenergy spectrum crucially depends on the value of  $\beta$ . Whereas irrational values of  $\beta$  lead to a self-similar spectrum, this is not the case for rational  $\beta$ . Experimentally, indications of this behaviour have been seen as a reduction in the critical temperature in superconducting networks at rational values

of  $\beta$  [15], as well as in measurements of the magnetoresistance [16] and the Hall conductance [17] in two-dimensional electron gases in superlattice structures. Furthermore, a Hofstadter butterfly structure was found in the transmission through a one-dimensional microwave resonator with appropriately chosen scatterers inserted [18]. Very recently, the use of optical lattices was suggested [19]: cold atoms moving on a closed path acquire a phase due to Raman transitions, thus simulating the external magnetic field of the originally considered system.

The peculiarity of a self-similar energy spectrum suggests to study the Hamiltonian (1) as a function of the potential strength  $\lambda$  while fixing  $\beta$  at an irrational value. Then, the potential is incommensurate with the underlying lattice and one obtains a quasiperiodic potential. Following Aubry and André [10], one may expect a phase transition from extended to localized states as  $\lambda$  is increased beyond a critical value of 2. However, later it was proved that somewhat stronger requirements need to be imposed on  $\beta$ . A necessary and sufficient condition for a phase transition to occur in the Aubry–André model is that  $\beta$  is a Diophantine number [20]. In the following, we will use the inverse of the golden mean,  $\beta = (\sqrt{5} - 1)/2$ , which is Diophantine and a common choice in studies of the Aubry–André model.

We remark that potential parameters in (1), which are common to both the Harper model and the Aubry–André model, have been of special interest. Diffusion properties have been related to properties of the energy spectrum [21] and a semi-Poisson energy level spacing distribution was found [22], thus hinting at the existence of a critical spectral statistics at  $\lambda = 2$  and  $\beta = (\sqrt{5} - 1)/2$ .

An important aspect of the Aubry–André model is the incommensurability of the periodic potential in (1), with respect to the underlying lattice that is guaranteed by the choice of  $\beta$  as an irrational number. Numerical studies, however, will in general have to be carried out on a finite lattice with periodic boundary conditions imposed to avoid undesirable boundary effects. In this case, the periodic potential is no longer truly incommensurate and caution has to be exercised when increasing the system size. The inverse of the golden mean is a convenient choice [23] because the convergents of its continued fraction representation are given by ratios of successive Fibonacci numbers defined by the recursion relation  $F_{n+1} = F_n + F_{n-1}$  with  $F_0 = 0$  and  $F_1 = 1$ . Therefore, if the system size is chosen as a Fibonacci number  $F_i$ , the period  $\beta$  in (1) can be approximated by  $F_{i-1}/F_i$ , which yields the inverse of the golden mean in the limit of large system sizes.

Both, the Hamiltonian (1) and its finite size approximations just discussed, possess a potential which is symmetric with respect to the site  $n = 0$ . Therefore, energy eigenstates may always be chosen as symmetric or antisymmetric. This not only presents conceptual but also technical advantages because it reduces the Hamiltonian to tridiagonal form even in the presence of periodic boundary conditions [24]. Since in this way much larger system sizes become accessible, we will always consider states of definite symmetry. It was checked that even for rather small system sizes the results do not change if the states of the other symmetry class are taken into account as well.

From the real-space representation (1) of the Aubry–André model, one can derive a dual model in momentum space [10]. This can be seen by introducing new basis states

$$\begin{aligned} |\bar{k}\rangle &= L^{-1/2} \sum_n \exp(i2\pi\bar{k}\beta n) |n\rangle \\ &= L^{-1/2} \sum_n \exp\left(i2\pi \frac{\bar{k}F_{i-1}}{L} n\right) |n\rangle, \end{aligned} \quad (2)$$

where the system size is given by  $L = F_i$ . Note that these states are eigenstates of the momentum operator not with eigenvalue  $\bar{k}$  but rather

$$k = \bar{k}F_{i-1} \bmod F_i. \quad (3)$$

Employing the states (2) allows us to rewrite the Hamiltonian (1) as

$$H = \frac{\lambda}{2} \left[ \sum_{\bar{k}} (|\bar{k}\rangle\langle\bar{k}+1| + |\bar{k}+1\rangle\langle\bar{k}|) + \frac{4}{\lambda} \sum_{\bar{k}} \cos(2\pi\beta\bar{k})|\bar{k}\rangle\langle\bar{k}| \right]. \quad (4)$$

The Hamiltonian (1) in real space is thus mapped onto a Hamiltonian of the same form in a permuted momentum space with the original potential strength  $\lambda$  replaced by  $4/\lambda$ . Of particular importance is the self-dual point  $\lambda = 2$  where the localization transition occurs.

For later purposes, it is useful to discuss in more detail the nearest-neighbour coupling between the momentum-type states (2). The momentum transfer experienced by a plane wave due to scattering by the incommensurate potential is  $\pm 2\pi F_{i-1}/L$ . As a consequence, the coupling present in (4) never couples adjacent momentum eigenvalues  $k$  for system sizes equal to or larger than 5. In fact, in most cases, the coupling will lead to momenta well separated from the original momentum. However, real energy eigenstates always contain pairs  $\pm k$  of momentum components with equal weight. Therefore, it may happen in special cases with momenta  $\pm 2\pi n/L$ , where  $2n$  is close to  $F_{i-1}$  or  $F_{i-2}$ , that the coupling due to the first term in (4) leads exactly to or close to the other momentum eigenvalue in the pair.

As this discussion demonstrates, the coupling in momentum space is quite complex and very different in nature from the nearest-neighbour coupling in real space. This observation will be of great importance for the phase-space behaviour and, in particular, for the appearance of a phase transition [5].

To attain a clearer picture of the duality of the Aubry–André model, we present in figures 1(a) and (b) the densities  $|\psi(x)|^2$  and  $|\tilde{\psi}(k)|^2$  in real and momentum spaces, respectively, as a function of the potential strength. Although the system size  $L = 55$  is quite small,  $\lambda = 2$  is clearly recognizable as a special potential strength. Approaching  $\lambda = 2$  in figure 1(a) from the right, one observes a broadening of the real-space density, which is related to the nearest-neighbour coupling in (1). The dual version can be seen in figure 1(b) to the left of  $\lambda = 2$ . However, instead of a broadening, this state taken from the middle of the band displays the generic behaviour of coupling to distant momentum values and it can clearly be seen how an increasing number of momenta become involved as  $\lambda = 2$  is approached. Of course, if on the vertical axis in figure 1(b) we plot  $\bar{k}$  as defined by (2) instead of the momentum  $k$ , the duality would imply that the two figures were exact mirror images of each other. The difference between figures 1(a) and (b) is therefore due to the reshuffling of momenta values according to (3). For example, the state  $n = \bar{k} = 41$  in a system of size  $L = F_i = 55$  turns into state  $19 \equiv 41 \cdot 34 \bmod 55$  in momentum space.

A more quantitative analysis can be given in terms of the inverse participation ratios in real and momentum space. For a state  $|\psi\rangle$ , we define the inverse participation ratio in real space as

$$P_x = \sum_n |c_n|^4 \quad (5)$$

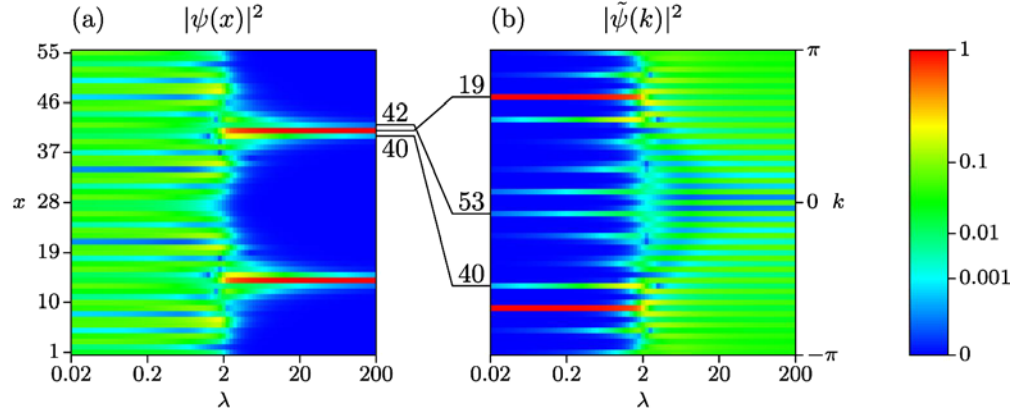


**Figure 1.** Real space (a) and momentum space (b) probability density as a function of the potential strength  $\lambda$  for an Aubry-André model of length  $L = 55$  and a state in the middle of the band. The corresponding colour scale is depicted on the right, where a value of one corresponds to the maximum value present in the respective plot. The lines connecting the two plots indicate for three examples the mapping from position eigenstates  $|n\rangle$  to momentum eigenstates  $|k\rangle$ .

with the coefficients  $c_n = \langle n|\psi\rangle$  normalized according to  $\sum_n |c_n|^2 = 1$ .  $P_x$  is a measure for the inverse number of sites occupied by the state as can be understood by regarding two limiting cases. If the state is localized on a single site  $\ell$ , we immediately find from  $c_n = \delta_{n,\ell}$  that  $P_x = 1$ . If, on the other hand, the state is distributed equally over  $N$  sites, we have  $c_n = N^{-1/2}$  and thus  $P_x = 1/N$ . Switching to the momentum space representation by means of

$$d_l = L^{-1/2} \sum_n \exp\left(i2\pi \frac{nl}{L}\right) c_n, \quad (6)$$

we define the inverse participation ratio in momentum space as

$$P_k = \sum_l |d_l|^4. \quad (7)$$

In the localized regime, i.e. for  $\lambda \rightarrow \infty$  in real space or  $\lambda \rightarrow 0$  in momentum space, one expects an inverse participation ratio of  $1/2$  reflecting the localization onto two sites for almost all symmetric and antisymmetric states. On the other hand, in the delocalized case, most states will exhibit a sinusoidal density profile which yields an inverse participation ratio of  $3/2L$ . Figures 2(a) and (b) depict the inverse participation ratios in real and momentum spaces, respectively, as a function of the potential strength. The curves exhibit a rather abrupt change at  $\lambda = 2$  even for a quite small system size of  $L = 144$ . In contrast with the densities shown in figure 1, the inverse participation ratios are perfectly dual, i.e. they obey  $P_x(\lambda) = P_k(4/\lambda)$ , because  $P_k$  is not sensitive to the permutation implied by (2). This will no longer hold true when we consider the situation in phase space.

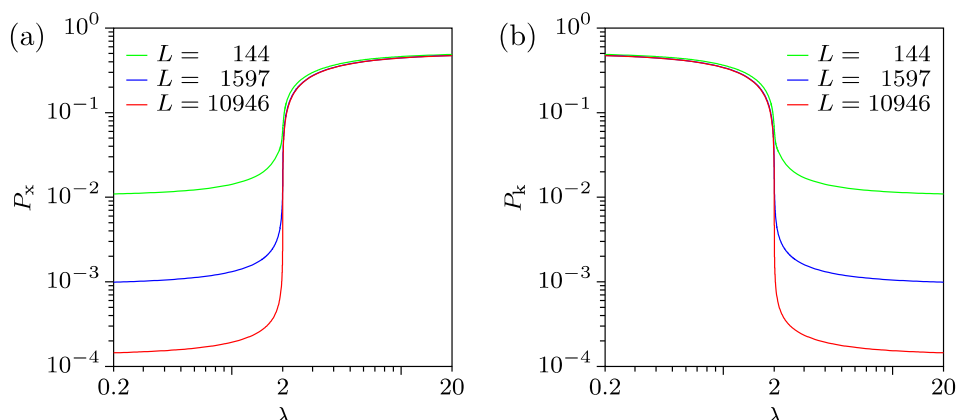


**Figure 2.** Inverse participation ratio in real space (a) and momentum space (b) as a function of the potential strength  $\lambda$  after averaging over all antisymmetric eigenstates. Results are shown for systems of size  $L = 144, 1597$  and  $10946$ . The two plots are mirror images of each other, thereby reflecting the duality of the Aubry–André model.

### 3. Phase-space concepts

In contrast with classical physics, quantum mechanics allows us to construct an infinite variety of phase-space distributions corresponding to different operator orderings [25]. All these distributions have to account for the Heisenberg uncertainty relation and therefore do not allow for a perfect localization in the phase space. In some cases, this leads to distributions which are in general not well behaved. The most convenient phase-space distribution for our purposes is the Husimi function [2, 3], which in quantum optics is commonly referred to as  $Q$  function [26, 27]. An important property of the Husimi function, namely the fact that it is positive-definite, is a direct consequence of its definition

$$\varrho(x_0, k_0) = |\langle x_0, k_0 | \psi \rangle|^2, \quad (8)$$

where the state  $|\psi\rangle$  is projected onto a minimal uncertainty state  $|x_0, k_0\rangle$  centred in phase space at position  $x_0$  and momentum  $k_0$ . In real space, the minimal uncertainty state is given by

$$\langle x | x_0, k_0 \rangle = \left( \frac{1}{2\pi\sigma^2} \right)^{1/4} \exp\left( -\frac{(x - x_0)^2}{4\sigma^2} + ik_0x + \frac{i}{2}k_0x_0 \right). \quad (9)$$

Whereas in applications in the context of quantum optics, the width  $\sigma$  is determined by the frequency of the electromagnetic field mode under consideration, in our case we are free to choose  $\sigma$ . An unbiased choice implies that the relative widths in the two directions,  $\Delta x/L$  and  $\Delta k/2\pi$ , should be equal. In addition, as a minimal uncertainty state, (9) satisfies  $\Delta x \Delta k = 1/2$ , which fixes the width of the coherent state to  $\sigma = \sqrt{L/4\pi}$ . As a consequence, the relative resolution increases as the system size is increased.

Figure 3(a) depicts an example of a Husimi function. Here, the dark blue spots indicate phase-space points where zeros of the Husimi function might be situated. It can be shown that

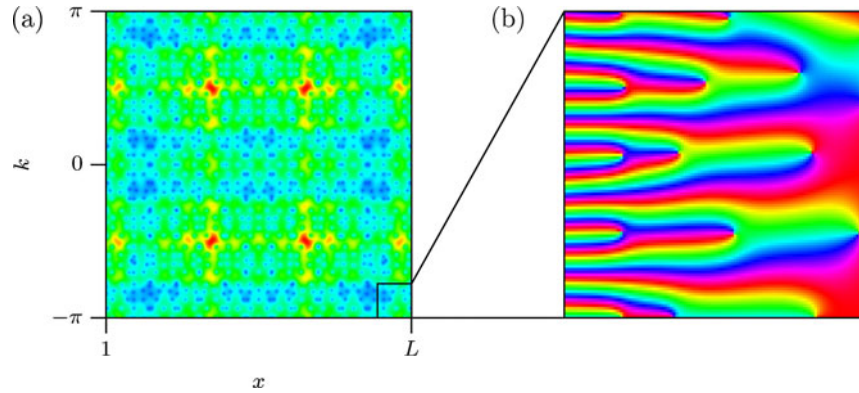


**Figure 3.** The Husimi function  $\varrho(x, k)$  for a state in the middle of the band and system size  $L = 987$  is depicted in (a) for the critical potential strength  $\lambda = 2$ . The lower right corner of phase space is expanded in (b) to show the phase of  $\langle x, k | \psi \rangle$  coded in colours. The zeros in this region of phase space can be recognized by a colour change around them covering the full spectrum.

the knowledge of the zeros is sufficient to uniquely define the complete Husimi function [28] (note that the definition of the Husimi function in [28] differs slightly from ours as long as  $L \gg \sigma$  is not satisfied). To distinguish between true zeros and mere dips in the Husimi function, it is useful to consider the behaviour of the phase of  $\langle x, k | \psi \rangle$ . Around a zero, the phase will change by multiples of  $2\pi$  depending on the multiplicity of the zero. This is shown in figure 3(b), where the phase has been coded in colour. Zeros are situated at points around which the colour changes through the whole spectrum.

Even for one-dimensional systems, i.e. two-dimensional phase space, the Husimi function contains a tremendous amount of information and it may be desirable to characterize a state in a more succinct way. We therefore generalize the definition of the inverse participation ratio given in section 2 to phase space and introduce [4, 29, 30]

$$P = \int \frac{dx dk}{2\pi} \varrho(x, k)^2. \quad (10)$$

This quantity can be viewed as a linearized version of the so-called Wehrl entropy [31]

$$S = - \int \frac{dx dk}{2\pi} \varrho(x, k) \ln[\varrho(x, k)]. \quad (11)$$

These and related quantities have frequently been used to characterize chaotic systems [32]–[36]. The inverse participation ratio (10) takes its maximum value,  $P = 1/2$ , for minimal uncertainty states, i.e. states optimally localized in phase space. All other states will therefore lead to values of  $P$  smaller than  $1/2$ .

The definition (10) seems to imply that the Husimi function  $\varrho(x, k)$  needs to be calculated first before the inverse participation ratio can be obtained. On the other hand, already the wave function  $\psi(x)$  contains the full information about a state. Indeed, making use of the definition

(8) of the Husimi function one may express the inverse participation ratio (10) in terms of the wave function as [37]

$$P = \frac{1}{8\sqrt{\pi}\sigma} \int du \left| \int dv \psi\left(\frac{u-v}{2}\right) \psi\left(\frac{u+v}{2}\right) \exp\left(-\frac{v^2}{8\sigma^2}\right) \right|^2. \quad (12)$$

Another approach to characterize the phase-space structure of a state consists in considering the marginal distributions of the Husimi function

$$\zeta(x) = \int \frac{dk}{2\pi} \varrho(x, k), \quad (13)$$

$$\eta(k) = \int dx \varrho(x, k). \quad (14)$$

An important ingredient of the phase-space approach is the Gaussian smearing present in the Husimi function which allows to obtain new insight into a problem [5]. Expressing the marginal distributions in terms of wave functions in real and momentum spaces reveals the presence of such a smearing:

$$\zeta(x) = \int dx' g_\sigma(x-x') |\psi(x')|^2, \quad (15)$$

$$\eta(k) = \int \frac{dk'}{2\pi} g_{1/2\sigma}(k-k') |\tilde{\psi}(k')|^2 \quad (16)$$

with

$$g_\Sigma(x) = \frac{1}{(2\pi\Sigma^2)^{1/2}} \exp\left(-\frac{x^2}{2\Sigma^2}\right). \quad (17)$$

On the basis of the marginal distributions (15) and (16), we can again define inverse participation ratios

$$P_\zeta = \int dx \zeta(x)^2, \quad (18)$$

$$P_\eta = \int \frac{dk}{2\pi} \eta(k)^2. \quad (19)$$

It turns out that for a Husimi function of Gaussian form, these inverse participation ratios of the marginal distributions and the inverse participation ratio in phase space are related by

$$P = P_\zeta P_\eta. \quad (20)$$

For other Husimi functions, this relation usually holds to a very good approximation [8], especially when the phase-space distribution does not contain structures associated with the classical limit of the model under consideration.

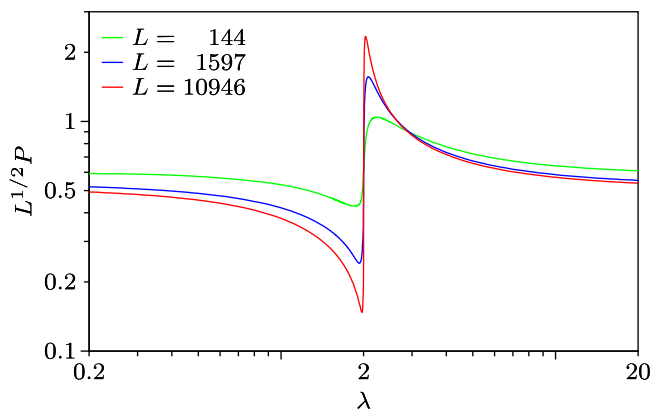


**Figure 4.** Inverse participation ratio (10) in phase space as a function of the potential strength  $\lambda$  after averaging over all antisymmetric eigenstates. Results are shown for systems of size  $L = 144, 1597$  and  $10946$ .

Within this second approach it is natural to define an entropy on the basis of the marginal distributions as

$$S[\zeta] = - \int dx \zeta(x) \ln [\zeta(x)], \quad (21)$$

$$S[\eta] = - \int \frac{dk}{2\pi} \eta(k) \ln [\eta(k)] \quad (22)$$

from which an entropy in phase space [8]

$$S[\varrho] \approx S[\zeta] + S[\eta] \quad (23)$$

can be constructed. As above, the inverse participation ratio (20) can be viewed as a linearization of the entropy (23). It should be noted that a comparison between the quantities by means of the structural entropy  $S_{\text{str}} = S + \ln P$  can yield interesting information as was shown in real space [38, 39] as well as in phase space [8]. In the following, we will not consider entropies but rather concentrate on the Husimi function (8) and the inverse participation ratios (10) and (20).

#### 4. Aubry–André model in phase space

The behaviour of the inverse participation ratio in phase space as a function of the potential strength  $\lambda$  is displayed in figures 4 and 5 (solid lines). Whereas in figure 4, the inverse participation ratio (10) is shown for different system sizes  $L = 144, 1597, 10946$ , the solid line in figure 5 represents the inverse participation ratio defined by the right-hand side of (20) for a system of size  $L = 1597$ . In both figures, an average over all antisymmetric eigenstates has been performed. A comparison of the two inverse participation ratios (10) and (20) for  $L = 1597$  shows that they are barely distinguishable within the linewidth, so that corrections to the product representation on the right-hand side of (20) are irrelevant here.

Starting from weak potential strengths, the average inverse participation ratio decreases until  $\lambda = 2$  is reached. While this holds true for most of the states, we will see later that exceptional

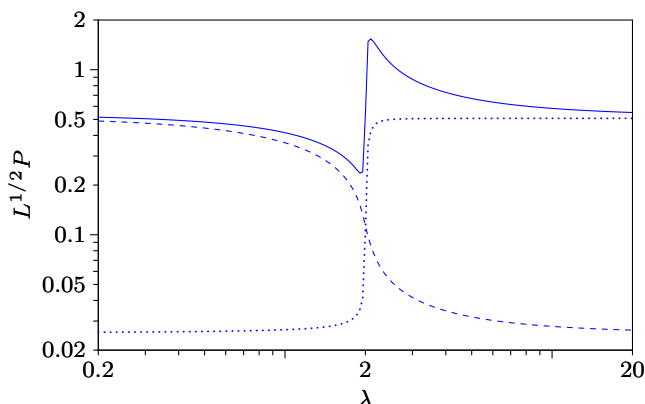


**Figure 5.** Inverse participation ratios based on marginal distributions are shown for a system of size  $L = 1597$  as a function of the potential strength  $\lambda$  after averaging over all antisymmetric eigenstates. The inverse participation ratios in real space (18) and momentum space (19) are represented by the dotted and broken line, respectively. Their product yields the inverse participation ratio in phase space (20) depicted as a solid line.

states exist which first show an increase in  $P$ . Even for these states, however,  $P$  will decrease close to  $\lambda = 2$ . The general behaviour of the inverse participation ratio for  $\lambda < 2$  reflects the spreading of the states in phase space with increasing potential strength. Around  $\lambda = 2$ , an abrupt change in the inverse participation ratio indicates a significant contraction of the phase-space distribution, which becomes more prominent with increasing system size. This feature announces the appearance of a phase transition in the thermodynamic limit. Beyond the phase transition, the Husimi function spreads again until all states localize at not more than two lattice sites.

It is intriguing to observe that in the inverse participation ratios in phase space there exist no obvious signs of the duality discussed in section 2, i.e.  $P(\lambda) \neq P(4/\lambda)$ . In figure 2, the duality had been manifest in the inverse participation ratios in real and momentum spaces. Phase-space quantities, such as the inverse participation ratio depicted in figures 4 and 5, contain both real- and momentum-space information and it would therefore be plausible to expect the inverse participation ratio to be symmetric with respect to  $\lambda = 2$ . Instead, the inverse participation ratio almost everywhere decreases with increasing  $\lambda$ , thus hinting at a dominant role of the momentum-space physics. This is supported by the inverse participation ratios (18) in real space and (19) in momentum space depicted in figure 5 by the dotted and broken line, respectively. The dependence of the inverse participation ratio in phase space on the potential strength follows the behaviour of the corresponding quantity in momentum space, except for the vicinity of the transition at  $\lambda = 2$  where the real-space properties dominate. The absence of the duality leads us to expect that interesting insights into the Aubry–André model beyond the results of section 2 can be gained from a phase-space analysis.

We can profit from the low dimensionality of the Aubry–André model to gain a better intuition for the phase-space behaviour by taking a look at the dependence on  $\lambda$  of the Husimi function itself. The Husimi function of a state in the middle of the band is shown in figure 6 for various values of the potential strength  $\lambda$ . For very weak potential, two horizontal stripes symmetrically placed with respect to  $k = 0$  indicate the presence of two counterpropagating

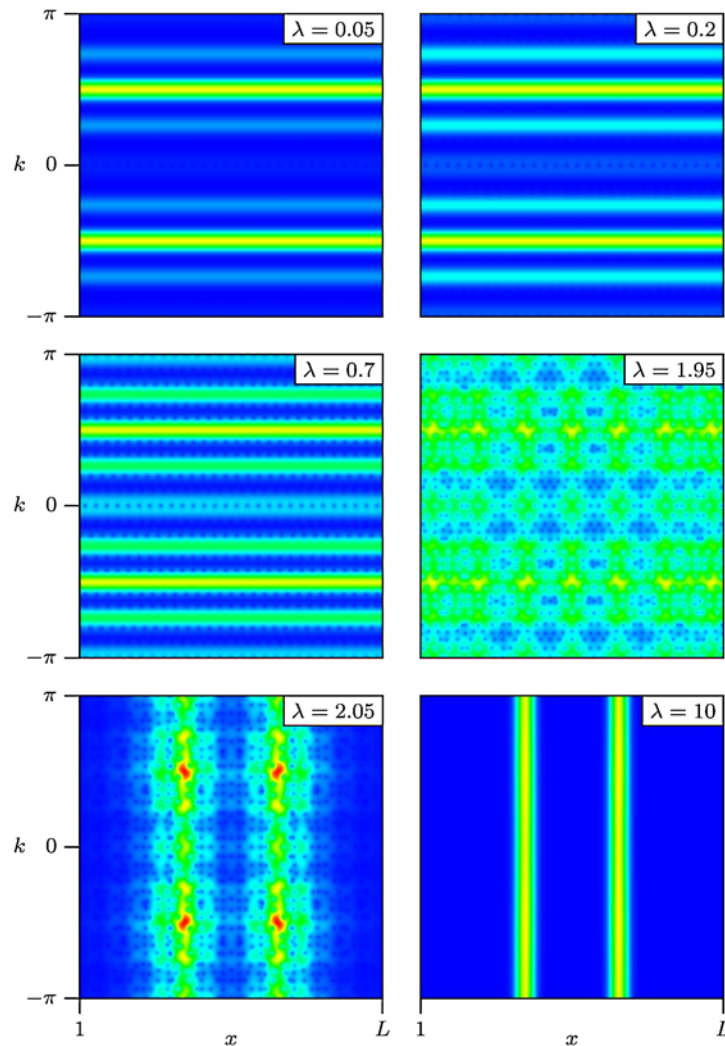


**Figure 6.** Evolution of the Husimi distribution as a function of the potential strength  $\lambda$  for the same eigenstate of the Aubry–André model as in figure 3, i.e. taken from the middle of the band for a system of size  $L = 987$ . The colour scale of figure 1 has been employed with a value of one corresponding to the maximum of the Husimi function over all potential strengths. (See [animation](#).)

plane waves. The width of the stripes arises from the projection onto a minimal uncertainty state and thus reflects the quantum nature of the state represented.

With increasing potential strength, additional stripes appear and gain in weight. This is consistent with the nearest-neighbour coupling in the dual form (4) of the Aubry–André Hamiltonian. Already the original stripes cover a range of momentum values so that the additional stripes appearing now have to be relatively far from the original momenta. As the potential strength increases further, more and more momentum eigenstates contribute to the state under consideration. In addition, beating phenomena occur which we will study in more detail below. Just before  $\lambda = 2$  is reached, the phase space is rather well covered by the Husimi function.

Around  $\lambda = 2$ , the phase-space picture changes drastically. Were the Husimi function, up to now, more or less homogeneous in spatial direction, it now becomes well localized. However, there is still a rather large degree of localization present also in momentum direction which is reflected by the large values of the inverse participation ratio in phase space in figure 4. The structure present in momentum direction finally disappears as the potential strength tends to infinity and we are left with the Husimi function of a state localized in most cases on two lattice sites.

Although we focus here on the Aubry–André model, it is instructive to compare with the Anderson model in one dimension. The only difference to the Aubry–André model consists in replacing the potential term in the Hamiltonian (1) by a random potential with uncorrelated on-site potentials distributed equally between  $-W/2$  and  $W/2$ . The dependence of the Husimi function on the potential strength  $W$ , as shown in figure 7, is qualitatively different from that for the Aubry–André model.

At weak random potential, the main change with increasing potential strength results in a contraction in spatial direction, leaving at intermediate disorder strength,  $W \approx 1$ , a Husimi function still well localized in momentum space and also localized in real space. This behaviour corresponds to an increase in the inverse participation ratio in phase-space reminiscent of what can be observed in figure 2(a) in real space for  $\lambda < 2$ . For larger potential strengths, the Husimi function changes very much similar to the case for the Aubry–André model. The phase-space distribution is already quite well localized in real space but, nevertheless, it is extended over several lattice sites as can be seen from the structure in momentum direction. The increasing spatial localization can be observed via the disappearance of the structure in momentum direction. This latter part of the evolution of the Husimi function is well described by the decrease in the inverse participation ratio in momentum space very much similar to that shown in figure 2(b) for the Aubry–André model. Thus, the inverse participation ratio for the Anderson model behaves very much as one would have expected for the Aubry–André model in view of its duality property. We now need to understand why the Aubry–André model in phase space behaves differently.

An important aspect of a phase-space description is the finite resolution in both, real and momentum spaces. A perfect resolution in one direction can only be bought at the expense of losing any resolution in the other direction. The finite resolution of the Husimi function should, however, not be viewed as a disadvantage but rather as an important aspect of the physical situation under study. We therefore have to analyse in some more detail the consequences of this finite resolution.

The main point to understand is the difference between the limits  $\lambda \rightarrow 0$  and  $\lambda \rightarrow \infty$  in the Aubry–André model. The duality implies that in both cases it is the nearest-neighbour interaction which causes the perturbation. However, for  $\lambda \rightarrow 0$ , the coupling, in general, does not occur between nearest neighbours in momentum space but in a permuted momentum space. Whereas for the inverse participation ratio in momentum space this did not matter, it does so in phase space where the resolution can only be finite. The relevance of the finite resolution is already evident from the inverse participation ratios in real and momentum spaces shown in figure 5 as dotted and broken line, respectively. Here, the duality observed in figure 2 no longer holds. In fact, the inverse participation ratios  $P_k$  defined in (7) and  $P_\eta$  defined in (19) differ. In contrast with  $P_k$ , the Gaussian smearing renders  $P_\eta$  sensitive to the permutation of momentum space associated with the duality transformation. We therefore have to distinguish situations where the momenta coupled are close or distant.

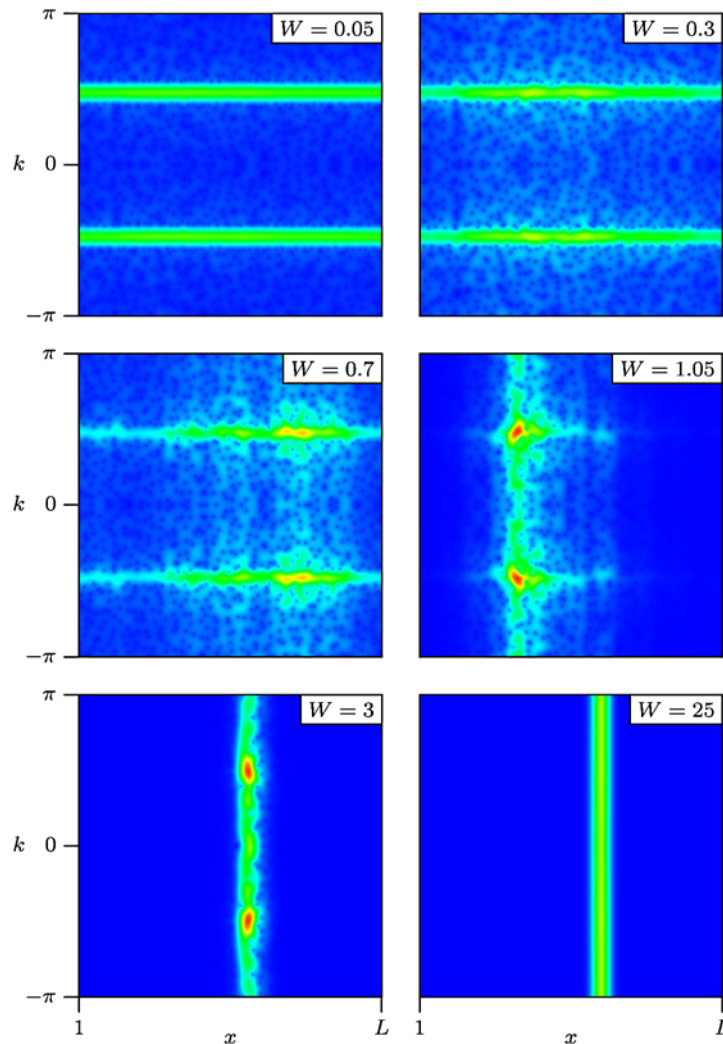


**Figure 7.** Evolution of the Husimi distribution as a function of the disorder strength  $W$  for an eigenstate of the Anderson model taken from the middle of the band for a system of size  $L = 987$ . The colour scale of figure 1 has been employed with a value of one corresponding to the maximum of the Husimi function over all disorder strengths. (See [animation](#).)

From the discussion of figure 6 we know already what happens in the case of coupling to distant momenta in the limit  $\lambda \rightarrow 0$ . The phase-space area occupied by the Husimi function will increase because additional momenta contribute and no large-scale structure in real space develops. Correspondingly, the inverse participation ratio will decrease with increasing coupling.

On the other hand, in the limit  $\lambda \rightarrow \infty$ , the coupling occurs between spatially close states, i.e. states which fall within the width of the Husimi function. In this case, the coupling does not contribute to a decrease in the inverse participation ratio in phase space because it does not even become visible in the real-space direction of phase space. However, a signature of this coupling appears in momentum space in form of a beating of the Husimi function. This arises from a superposition of the form  $\exp[ikx_0] + \exp[ik(x_0 + \delta)]$  if the state is localized at sites  $x_0$  and  $x_0 + \delta$

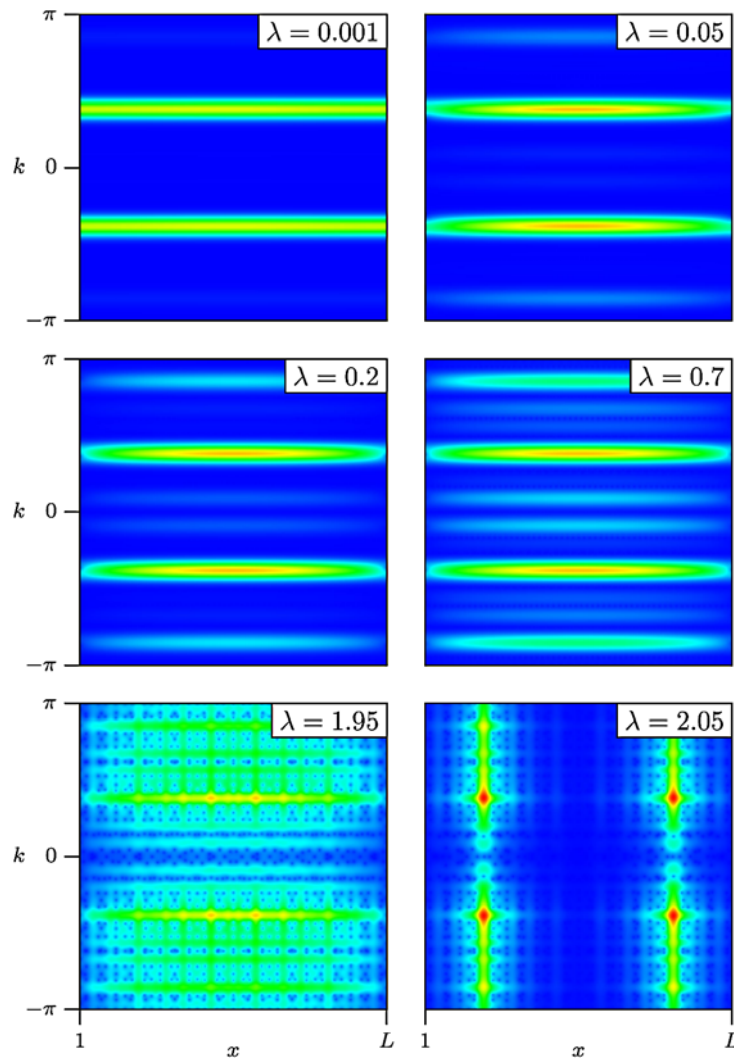


**Figure 8.** Evolution of the Husimi distribution as a function of the potential strength  $\lambda$  for a special eigenstate of the Aubry–André model of size  $L = 987$ , where the dominant coupling by the weak potential occurs to nearest neighbours in momentum space. The colour scale of figure 1 has been employed with a value of one corresponding to the maximum of the Husimi function over all potential strengths. (See [animation](#).)

with  $\delta$  smaller than the width  $\sigma$  of the minimal uncertainty state employed to determine the Husimi function.

Such a scenario can be realized also at weak potential for special states where the leading coupling due to the potential occurs close to momentum components of the state at  $\lambda = 0$ . According to what we just have seen for  $\lambda \rightarrow \infty$ , such a state will first contract in real space as  $\lambda$  increases. This corresponds to an increase in the inverse participation ratio  $P$  as mentioned earlier. However, as can be seen in figure 8, the state will eventually spread in momentum space before reaching the critical potential strength  $\lambda = 2$  and thus follow the general scenario of the localization transition of the Aubry–André model. In contrast, for small  $\lambda$ , this special state

behaves rather like an eigenstate of the Anderson model, where the coupling to nearest neighbours is predominant [5, 7].

From this discussion, it becomes clear that the duality of the Aubry–André model does not manifest itself in phase space in an obvious way. The main reason is that at small  $\lambda$  the nearest-neighbour coupling between states (2) corresponds to a coupling between distant states in momentum space. As a consequence, both for small and large  $\lambda$ , momentum space dominates the behaviour in phase space and the Husimi function tends to spread with increasing potential strength. It is only very close to  $\lambda = 2$  that real space becomes important where the Husimi function contracts with increasing  $\lambda$ . This is supported by a comparison of the solid and dotted lines in figure 5.

The existence of a metal–insulator transition, with the abrupt contraction of the Husimi distribution as its signature in phase space, can now be understood. In the limits  $\lambda \rightarrow 0$  and  $\infty$ , the Husimi distribution of a generic state has the same form, consisting of two stripes either in real- or momentum-space direction. As we have seen, the Husimi distribution is spreading as  $\lambda$  increases from 0 and as it approaches  $\infty$ . This is only possible, if for some intermediate value of  $\lambda$ , a contraction of the Husimi distribution occurs. With increasing system size, the phase-space filling below  $\lambda = 2$  slightly increases and, more importantly, the phase space occupied by the states just above the critical value of  $\lambda$  will decrease because of the increasing relative resolution of the Husimi function. In the thermodynamic limit, this leads to an abrupt contraction of the phase-space distribution as an indication of the phase transition in the Aubry–André model.

Such a scenario should also be expected for the Anderson model in two and higher dimensions, where a direct visualization of the Husimi function is unfortunately not possible. However, a study of the inverse participation ratio reveals that the overall behaviour of this quantity as a function of the potential strength for the Aubry–André model and the Anderson model in two and higher dimensions is very similar [7]. A noteworthy difference between the two models is the existence, for the Anderson model, of a broad region of disorder strengths below the phase transition, where the phase space is well covered and which can be related to the existence of a diffusive regime [4]. A corresponding plateau in the inverse participation ratio is not found in the Aubry–André model (cf figure 4), which is consistent with the absence of a diffusive regime in that model.

Apart from this detail, the Aubry–André model and the Anderson model in two and higher dimensions display the same behaviour. In particular, at small potential strengths, the inverse participation ratio decreases with increasing potential strength. In fact, the physical picture of the momentum coupling at weak potential developed for the Aubry–André model works also for the Anderson model. Whereas in one dimension, momentum eigenstates close in energy are also close in momentum, this is not the case in two and higher dimensions where energetically degenerate momentum eigenstates lie on hypersurfaces in momentum space. Our phase-space considerations thus offer an explanation for the absence of a phase transition in the one-dimensional Anderson model [7].

## 5. Conclusion

The existence of a metal–insulator transition in one dimension makes the Aubry–André model particularly suited for a phase-space study over the full range of potential strengths. An intuitive picture of the evolution of individual states across the transition is provided by the Husimi function

and inverse participation ratios have been employed to quantify the phase-space spreading of the states. The scenario found for the Aubry–André model is fundamentally different from that for the one-dimensional Anderson model where no phase transition occurs. A comparison of the two models points towards the relevance of the coupling between momentum eigenstates for the existence of a phase transition. With respect to this coupling, the Aubry–André model resembles very much the Anderson model in two and higher dimensions and thus provides additional insight into the dependence of the Anderson transition on dimension.

## Acknowledgments

The authors thank D Weinmann for stimulating discussions. This work was supported by the Sonderforschungsbereich 484 of the Deutsche Forschungsgemeinschaft. I V acknowledges financial support from the Alexander von Humboldt Foundation, the Hungarian Academy of Sciences and the OTKA grants No. T034832, T042981 and T046303. The numerical calculations were carried out partly at the Leibniz-Rechenzentrum München.

## References

- [1] Weinmann D, Kohler S, Ingold G-L and Hänggi P 1999 *Ann. Phys. (Lpz)* **8** SI277
- [2] Husimi K 1940 *Proc. Phys. Math. Soc. Japan* **22** 264
- [3] Lee H-W 1995 *Phys. Rep.* **259** 147
- [4] Wobst A, Ingold G-L, Hänggi P and Weinmann D 2002 *Eur. Phys. J. B* **27** 11
- [5] Ingold G-L, Wobst A, Aulbach C and Hänggi P 2002 *Eur. Phys. J. B* **30** 175
- [6] Ingold G-L, Wobst A, Aulbach C and Hänggi P 2003 *Lect. Notes Phys.* **630** 85
- [7] Wobst A, Ingold G-L, Hänggi P and Weinmann D 2003 *Phys. Rev. B* **68** 085103
- [8] Varga I and Pipek J 2003 *Phys. Rev. E* **68** 026202
- [9] Anderson P W 1958 *Phys. Rev.* **109** 1492
- [10] Aubry S and André G 1980 *Ann. Israel Phys. Soc.* **3** 133
- [11] Cycon H L, Froese R G, Kirsch W and Simon B 1987 *Schrödinger Operators* (Berlin: Springer)
- [12] Harper P G 1955 *Proc. Phys. Soc. A* **68** 874
- [13] Peierls R 1933 *Z. Phys.* **80** 763
- [14] Hofstadter D R 1976 *Phys. Rev. B* **14** 2239
- [15] Pannetier B, Chaussy J, Rammal R and Villegier J C 1984 *Phys. Rev. Lett.* **53** 1845
- [16] Schlösser T, Ensslin K, Kotthaus J P and Holland M 1996 *Europhys. Lett.* **33** 683
- [17] Albrecht C, Smet J H, von Klitzing K, Weiss D, Umansky V and Schweizer H 2001 *Phys. Rev. Lett.* **86** 147
- [18] Kuhl U and Stöckmann H-J 1998 *Phys. Rev. Lett.* **80** 3232
- [19] Jaksch D and Zoller P 2003 *New J. Phys.* **5** 56
- [20] Jitomirskaya S Ya 1999 *Ann. Math.* **150** 1159
- [21] Piéchon F 1996 *Phys. Rev. Lett.* **76** 4372
- [22] Evangelou S N and Pichard J-L 2000 *Phys. Rev. Lett.* **84** 1643
- [23] Kohmoto M 1983 *Phys. Rev. Lett.* **51** 1198
- [24] Thouless D J 1983 *Phys. Rev. B* **28** 4272
- [25] Hillery M, O’Connell R F, Scully M O and Wigner E P 1984 *Phys. Rep.* **106** 121
- [26] Cahill K E and Glauber R J 1969 *Phys. Rev.* **177** 1882
- [27] Schleich W P 2001 *Quantum Optics in Phase Space* (New York: Wiley-VCH)
- [28] Leboeuf P and Voros A 1990 *J. Phys. A: Math. Gen.* **A 23** 1765
- [29] Sugita A and Aiba H 2002 *Phys. Rev. E* **65** 036205
- [30] Sugita A 2003 *J. Phys. A: Math. Gen.* **36** 9081

- [31] Wehrl A 1979 *Rep. Math. Phys.* **16** 353
- [32] Gu Y 1990 *Phys. Lett. A* **149** 95
- [33] Mirbach B and Korsch H J 1995 *Phys. Rev. Lett.* **75** 362
- [34] Gorin T, Korsch H J and Mirbach B 1997 *Chem. Phys.* **217** 145
- [35] Gnutzmann S and Życzkowski K 2001 *J. Phys. A: Math. Gen.* **34** 10123
- [36] Korsch H J and Leyes W 2002 *New J. Phys.* **4** 62
- [37] Manfredi G and Feix M R 2000 *Phys. Rev. E* **62** 4665
- [38] Pipek J and Varga I 1992 *Phys. Rev. A* **46** 3148
- [39] Pipek J and Varga I 1994 *Int. J. Quantum Chem.* **51** 539